JVI Accepted Manuscript Posted Online 20 February 2019
J. Virol. doi:10.1128/JVI.00030-19

PPAR-γ in macrophages limits pulmonary inflammation and promotes host recovery following respiratory viral infection

Su Huang[a, b], Bibo Zhu[a, b], In Su Cheon[a, b], Nick P. Goplen[a], Li Jiang[a, b], Ruixuan Zhang[a], R. Stokes Peebles Jr.[c], Matthias Mack[d], Mark H. Kaplan[b], Andrew H. Limper[a] and Jie Sun[a, b]#

[a]Thoracic Diseases Research Unit, Division of Pulmonary and Critical Care Medicine, Department of Medicine, Department of Immunology, Mayo Clinic College of Medicine and Science
[b]HB Wells Pediatric Research Center, Department of Pediatrics, Indiana University School of Medicine
[c]Department of Medicine, Vanderbilt University Medical Center
[d]Department of Nephrology, University Hospital Regensburg, Germany

Running title: PPAR-γ regulates influenza diseases and recovery

#Corresponding author: Jie Sun, Sun.Jie@mayo.edu.

S Huang and B Zhu contributed equally to this work

ABSTRACT

Alveolar macrophages (AM) play pivotal roles in modulating host defense, pulmonary inflammation and tissue injury following respiratory viral infections. However, the transcriptional regulation of AM function during respiratory viral infections is still largely undefined. Here we have screened the expression of 84 transcription factors in AM in response to influenza A virus (IAV) infection. We found that the transcription factor PPAR-γ was downregulated following IAV infection in AM through type I interferon (IFN)-dependent signaling. PPAR-γ expression in AM was critical for the suppression of exaggerated antiviral and inflammatory responses of AM following IAV and respiratory syncytial virus (RSV) infection. Myeloid PPAR-γ deficiency resulted in enhanced host morbidity and increased pulmonary inflammation following both IAV and RSV infections, suggesting that macrophage PPAR-γ is vital for restricting severe host disease development. Using approaches to selectively deplete recruiting monocytes, we demonstrated that PPAR-γ expression in resident AM was likely important in regulating host disease development. Furthermore, we showed that PPAR-γ was critical for the expression of wound healing genes in AM. As such, myeloid PPAR-γ deficiency resulted in impaired inflammation resolution and defective tissue repair following IAV infection. Our data have suggested a critical role of PPAR-γ expression in lung macrophages in modulating pulmonary inflammation, the development of acute host diseases and the proper restoration of tissue homeostasis following respiratory viral infections.

IMPORTANCE: Respiratory viral infections, like IAV and respiratory syncytial virus (RSV) infections, impose great challenges to the public health. Alveolar macrophages (AM) are lung resident immune cells that play important roles in protecting the host against IAV and RSV infections. However, the underlying molecular mechanisms by which AM modulating host inflammation, disease development and tissue recovery are not very well understood. Here we identify that PPAR-γ expression in AM is crucial to suppress pulmonary inflammation and diseases, and to promote fast host recovery from IAV and RSV infections. Our data suggest that targeting macrophage PPAR-γ may be a promising therapeutic option in the future to suppress acute inflammation and simultaneously promote recovery from severe diseases associated with respiratory viral infections.

INTRODUCTION

Acute respiratory viral infections, such as influenza A virus (IAV) and respiratory syncytial virus (RSV) infections, cause severe morbidity and mortality, and are among leading causes of death in children and the elderly (1, 2). Particularly, IAV virus infection kills ~500,000 people globally and up to 50,000 people in the United States each year (3). In addition to seasonal outbreaks, pandemic IAV viruses occasionally emerge and can cause catastrophic illness and widespread death. Current strategies for IAV prevention and treatment include yearly vaccination and anti-viral drugs. However, frequent changes in the surface antigens of IAV virus due to antigenic shift and drift can allow IAV to escape antibody-mediated immunity following vaccination (4, 5). Anti-viral treatment is generally only effective during a very short time period early after IAV infection. Furthermore, many circulating IAV strains have developed resistance to the current antiviral drugs (6). Thus, there is urgent need to better understand the pathophysiology and the protective immune responses to IAV infection for the development of future preventive and therapeutic means.

The disease pathogenesis associated with IAV infection results from a combination of the deleterious effects of virus replication and the host innate and adaptive immune response associated with control and ultimately clearance of virus (7, 8). The major contribution of the host response to lung injury during IAV infection is exemplified by the immune-mediated lung inflammation and injury associated with infections with the 1918 pandemic IAV or the highly pathogenic H5N1 avian IAV. The inability to control the host responses in these infections results in excessive inflammatory cell infiltration into the lungs and overproduction of pro-inflammatory mediators ((9, 10).

As important components of innate immunity, tissue macrophages and monocyte populations are heterogeneous multifunctional immune sentinel cells important in modulating tissue homeostasis, inflammation, injury and repair (11-15). The main macrophage population in the respiratory tract is alveolar macrophages (AM) that play important roles in lung homeostasis and pulmonary anti-microbial defense (16, 17). Compared to other tissue macrophages, monocytes and monocyte-derived cells, AM have distinct functions and phenotypes that include high autofluorescence, low CD11b expression, and high expression of CD11c and Siglec-F (16, 18). AM precursors develop mainly from fetal monocytes, which seed the lung prior to birth, and massively expand and develop into mature macrophages in response to GM-CSF and TGF-β after birth (18-20). A number of factors including PPAR-γ, mTORC1, phosphoinositide kinase PIKfyve and L-plastin were also recently shown to be important in AM development and function (19, 21-24). Interestingly, AM appear to be essential for the protection against

IAV and other respiratory viral infections (25-31) . To this end, AM were identified as a major cellular source of the antiviral cytokines, type I interferons (IFNs) (29). Furthermore, AM can phagocytize virus and virus infected cells, clear cellular debris and exudates, and protect alveolar type I cells (ATI) from infection, thereby suppressing the development of lethal inflammation and injury during IAV infection (25-31). AM, particularly AM undergoing alternative polarization (M2), have also been implicated in the repair of damaged tissues following IAV infection (32). However, the underlying molecular mechanisms regulating the protective function of AM against respiratory viral infections remain to be fully elucidated.

PPAR-γ is a nuclear transcription factor, usually forming heterodimer with RXR (retinoid X receptor) which recruit different co-activators or co-repressors to form a complex binding to PPAR-responsive regulatory elements in the genome to modulate the expression of genes involved in adipogenesis, lipid metabolism and inflammation (33). PPAR-γ has been shown to be vital for M2 polarization and the restriction of excessive production of inflammatory factors (34, 35), although the roles of PPAR-γ in regulating macrophage inflammatory responses against viral infections have not been explored. AM constitutively express high levels of PPAR-γ (19). Mice with *lox*P-flanked alleles encoding PPAR-γ (*Pparg*$^{fl/fl}$) and with CD11c-driven expression of Cre recombinase (Cd11c–cre) that is efficiently expressed in fetal monocytes, exhibit severe defects in the AM compartment, suggesting that PPAR-γ is essential for AM development from fetal monocytes (19). Interestingly, prophylactic or therapeutic treatment of mice with natural or synthetic ligands which activate PPAR-γ resulted in diminished host morbidity and mortality during IAV infection (36-40) . However, the cellular and molecular mechanisms by which PPAR-γ agonists promote host protection against IAV infection have not been defined. In addition, the physiological and cell type-specific function of PPAR-γ in response to endogenous ligands during IAV infection are currently unknown.

In this report, we demonstrated that PPAR-γ was down-regulated in AM via IFNs following IAV infection. PPAR-γ repressed macrophage pro-inflammatory responses and promoted the expression of wound healing gene programs independent of M2 polarization, thereby modulating lung inflammation, host morbidity and tissue repair. We further showed that PPAR-γ expression and function in AM were likely important in dictating host diseases and recovery from respiratory viral infection.

RESULTS

IAV infection downregulates PPAR-γ expression in macrophages through IFNs

AM are important in regulating antiviral immunity and injury. However, the molecular mechanisms regulating AM responses to viral infection are still not well understood. To explore the transcriptional regulation of AM responding to viral infection, we infected WT AM with IAV PR8 (IAV, 10 MOI) *in vitro* and then determined the expression of 84 transcription factors (TFs) following overnight culture using Qiagen RT^2-PCR array. We found that a numbers of TFs involved in antiviral innate immunity were upregulated, while several TFs including *Pparg* were downregulated in AM following IAV infection (Figure 1 A and B). Quantitative PCR results also showed that *Pparg* was downregulated in AM following IAV infection (Figure 1 C). Western blot analysis confirmed decreased PPAR-γ at the protein level in IAV infected AM (Figure 1 D). To determine whether IAV infection downregulates *Pparg* in AM *in vivo*, we sorted AM ($CD11c^+$/Siglec F^+) from the lungs of uninfected (day 0) or IAV-infected mice (4, 6, 10 or 15 days post infection (d.p.i.)) and examined *Pparg* expression by realtime RT-PCR (Figure 1 E). We found that IAV infection diminished *Pparg* expression in AM, particularly at 6 d.p.i. (Figure 1 E). Western blot analysis confirmed that AM isolated from IAV-infected mice (6 d.p.i.) exhibited decreased PPAR-γ protein levels compared to AM isolated from uninfected mice (Figure 1 F). IAV infection triggers the production of anti-viral cytokines type I IFNs by AM (6). We next examined whether type I IFNs were involved in the regulation of PPAR-γ expression in AM. We found that IFN-α treatment suppressed PPAR-γ expression in AM (Figure 1 G). Next, we infected AM with IAV and then blocked type I IFN signaling with the inclusion of IFNAR1 blocking antibody (α-IFNAR1) in culture. We found that α-IFNAR1 treatment abolished IAV-induced suppression of *Pparg* expression in AM (Figure 1H). Similarly, α-IFNAR1 treatment abolished Poly IC induced suppression of *Pparg* expression in AM (Figure 1H). Together, these data suggest that IAV infection inhibited PPAR-γ expression in AM through IFN signaling. Consistent with the notion, we found that STAT1 could bind to *Pparg* locus following IFN-α treatment, suggesting that STAT1 activation following IFN signaling may directly modulate *Pparg* transcription in AM (Figure 1I).

PPAR-γ suppresses antiviral inflammation, but does not regulate M2 genes following infection

PPAR-γ is required for AM development because the deletion of PPAR-γ in $CD11c^+$ cells ($Pparg^{\Delta CD11c}$) resulted in impaired AM generation (Figure 2A and (19)). However, compared to CD11c-cre, Lyz2-cre expression in fetal monocytes is incomplete (19). As the result, Lyz2-cre driven PPAR-γ deficiency ($Pparg^{\Delta Lyz2}$) in AM resulted in relatively normal AM development (Figure 2A and (19). In comparison to the severe defects of AM development and maturation (evidenced by dramatic increase of CD11b (19)) observed in $Pparg^{\Delta CD11c}$ mice, $Pparg^{\Delta Lyz2}$ mice had comparable percentages of AM and only slightly

159 increased CD11b expression compared to those of control mice, suggesting that AM development and
160 maturation were relatively normal in *Pparg*$^{\Delta Lyz2}$ mice (Figure 2A). Nevertheless, Lyz2-cre is able to
161 mediate gene recombination in adult AM compartments and AM from adult *Pparg*$^{\Delta Lyz2}$ mice exhibited
162 impaired PPAR-γ expression (Figure 2 B and (30)). We therefore used AM from littermate control
163 (*Pparg*$^{fl/fl}$, WT) or *Pparg*$^{\Delta Lyz2}$ mice for our further analysis on the roles of PPAR-γ in regulating AM
164 function during respiratory viral infections. We first isolated AM from uninfected control or *Pparg*$^{\Delta Lyz2}$
165 mice, and infected the AM with IAV *in vitro* as in Figure 1. Following infection, WT and *Pparg*$^{\Delta Lyz2}$ AM
166 showed relatively comparable levels of viability (data not shown). We then examined the expression of
167 type I IFNs, inflammatory cytokines and M2 genes in control or PPAR-γ-deficient AM following IAV
168 infection. We found that PPAR-γ deficiency enhanced the expression of *Ifna4*, *Ifnb1*, *Tnf*, *Il1b* and *Ccl2*
169 expression, but did not affect the expression of *Retnla* (encoding RELM-α protein) and *Arg1* (encoding
170 Arginase 1 protein) (Figure 2C). These data suggest that PPAR-γ suppressed AM antiviral and
171 inflammatory responses, but did not change macrophage polarization following IAV infection. We next
172 infected control or *Pparg*$^{\Delta Lyz2}$ mice with IAV and then sorted AM from the lungs of infected mice at 1 or
173 3 d.p.i. We found that PPAR-γ deficient AM exhibited enhanced type I IFN and inflammatory gene
174 expression, but showed similar levels of *Retnla* and *Arg1* expression compared to those of control AM at
175 3 d.p.i. (Figure 2D). These data suggest PPAR-γ functioned to inhibit antiviral and inflammatory
176 responses, but did not regulate M2 polarization following IAV infection.
177
178 **Myeloid PPAR-γ suppresses lung inflammation, host morbidity and mortality**
179 To explore PPAR-γ expression in macrophages in regulating host antiviral responses and disease
180 development following IAV infection, we infected control or *Pparg*$^{\Delta Lyz2}$ mice with IAV and examined
181 host mortality, morbidity, viral replication and inflammatory responses at different days post infection.
182 Compared to control mice, *Pparg*$^{\Delta Lyz2}$ mice had enhanced host mortality and morbidity, and delayed
183 weight recovery following IAV infection (Figure 3 A, B). We examined the kinetics of IAV replication in
184 the respiratory tract using plaque forming unit (pfu) assay and found that *Pparg*$^{\Delta Lyz2}$ mice exhibited
185 significant increased virus titers early days following IAV infection (4 d.p.i.) compared to control mice
186 (Figure 3C). However, *Pparg*$^{\Delta Lyz2}$ mice had comparable viral titers at 7 d.p.i. and most of the mice cleared
187 their infectious virus around 10 d.p.i. (3 out of 11 mice exhibited detectable viruses in control or
188 *Pparg*$^{\Delta Lyz2}$ bronchoalveolar lavage fluid (BAL)) (Figure 3 C). Thus, *Pparg*$^{\Delta Lyz2}$ mice showed similar viral
189 clearance kinetics as control mice and suggest that the enhanced morbidity and mortality observed in
190 *Pparg*$^{\Delta Lyz2}$ mice was not merely due to the failure of viral clearance. Consistent with the viral clearance

data, we found that *Pparg*$^{\Delta Lyz2}$ mice exhibited comparable levels of IAV-specific CD8^{+} T cell responses (both H2d^{b} NP$_{366-374}$ tetramer^{+} and H2d^{b} PA$_{224-233}$ tetramer^{+}) at 7, 10 and 15 d.p.i. (Figure 3D).

Next, we measured lung inflammatory cytokine (CCL2 and TNF-α) levels in the BAL at different days following IAV infection to determine whether *Pparg* expression in myeloid cells regulates pulmonary inflammation. We found that *Pparg*$^{\Delta Lyz2}$ mice had significant higher CCL2 and TNF-α levels at early days post IAV infection (i.e. 1 or 3 d.p.i.) (Figure 3E). Notably, although the differences did not reach statistical significance, *Pparg*$^{\Delta Lyz2}$ mice showed trend of increased CCL2 protein levels in the BAL at 7, 10 or 15 d.p.i., indicating that *Pparg*$^{\Delta Lyz2}$ mice may have modest increased pulmonary inflammation at later days post infection. To this end, we used a more sensitive approach to examine inflammatory gene expression in the lungs of control or *Pparg*$^{\Delta Lyz2}$ mice by Qiagen RT^{2}-PCR array. We found that lungs of *Pparg*$^{\Delta Lyz2}$ mice exhibited altered expression of inflammation-related genes including higher expression of a number of pro-inflammatory genes (such as *Il6*, *Cxcl1* and *Fos*) at day 10 d.p.i. (Figure 3 F). Taken together, these data suggest that myeloid PPAR-γ deficiency leaded to enhanced early viral replication, exuberant inflammatory reaction and increased severity of host sickness.

Myeloid PPAR-γ inhibits inflammation and morbidity during RSV infection

To examine whether PPAR-γ controls AM inflammatory responses to other virus infection, we infected isolated AM from control or *Pparg*$^{\Delta Lyz2}$ mice with RSV, a virus that affects millions of children. Similar to what we have observed following IAV infection (Figure 2C), we found that PPAR-γ deficiency enhanced *Ifna4*, *Ifnb1*, *Tnf*, *Il1b and Ccl2* expression following RSV (line 19, 10 MOI) infection *in vitro*, suggesting that PPAR-γ also controls antiviral and inflammatory responses against RSV infection (Figure 4A). We then infected control or *Pparg*$^{\Delta Lyz2}$ mice with RSV (line 19) and examined host morbidity and lung inflammatory responses. We found that myeloid PPAR-γ deficiency increased weight loss following RSV infection (Figure 4 B). We also found that *Pparg*$^{\Delta Lyz2}$ mice had enhanced inflammatory innate immune cells (neutrophils and monocytes) present in the lungs at 4 d.p.i. (Figure 4C), suggesting that *Pparg*$^{\Delta Lyz2}$ mice had higher pulmonary inflammation compared to control mice. Consistently, BAL of *Pparg*$^{\Delta Lyz2}$ mice had higher TNF-α and IL-1β levels compared to those of control mice at 4 d.p.i. (Figure 4D). Thus, myeloid PPAR-γ was required for the suppression of exuberant host inflammation and exaggerated morbidity following RSV infection. These data suggest that macrophage PPAR-γ may restrict host disease development in a broad spectrum of respiratory viral infections.

PPAR-γ expression in resident AM is likely required for controlling host disease development

223 Lysozymes are widely expressed in myeloid cells including neutrophils, monocytes and macrophages. We
224 crossed Lyz2-cre mouse with a cre reporter strain R26R-eYFP mouse to examine Cre deletion in the
225 myeloid compartment. In agreement with previous report (35), we observed Lyz2-cre activity in majority
226 of alveolar macrophages and neutrophils, partially in CD11b^{+} monocytes/macrophages (Figure 5A).
227 Western-blot analysis on sorted myeloid cell populations isolated from the lungs revealed that AM
228 expressed high levels of PPAR-γ and lung CD11b^{+} monocyte/macrophage population expressed
229 comparatively lower levels of PPAR-γ (Figure 5B), while neutrophils did not express detectable PPAR-γ,
230 which is consistent with previous reports (35) (Figure 5B). To explore the potential roles of PPAR-γ in
231 regulating inflammation of AM, monocytes/monocyte-derived macrophages and/or epithelial cells, we
232 sorted AM, CD11b^{+} monocytes/macrophages and CD45^{-} (mainly epithelial cells) from IAV-infected
233 lungs of control or *Pparg*$^{\Delta Lyz2}$ mice at 1 and 3 d.p.i. and examined inflammatory cytokine expression. We
234 found that elevated *Tnf* and *Ccl2* expression was mainly observed in AM, but not in CD11b^{+}
235 monocytes/macrophages nor in CD45^{-} cells (Figure 5C). We next explored the relative contributions of
236 PPAR-γ in AM and monocytes/monocyte-derived macrophages in controlling host disease development
237 during IAV infection. To this end, we crossed *Pparg*$^{\Delta Lyz2}$ mice to *Ccr2*$^{-/-}$ mice to block monocyte traffic to
238 the infected lungs (40-43). We found that, compared to *Ccr2*$^{-/-}$/*Pparg*$^{fl/fl}$ mice, *Ccr2*$^{-/-}$/*Pparg*$^{\Delta Lyz2}$ mice lost
239 more weight and exhibited delayed recovery (Figure 5D), suggesting that enhanced disease development
240 in *Pparg*$^{\Delta Lyz2}$ mice is independent of monocytes or monocyte-derived cells. We next assessed whether
241 treatment of anti-CCR2 (MC21 mAb), which selectively depletes recruiting monocytes (44) could affect
242 host morbidity in *Pparg*$^{\Delta Lyz2}$ mice. As reported (43), MC21 treatment greatly decreased monocyte
243 infiltration to the lung (Figure 5E). However, MC21 treatment did not significantly alter host weight loss
244 in neither control nor *Pparg*$^{\Delta Lyz2}$ mice (Figure 5F), again suggesting that monocytes are dispensable for
245 phenotypes observed in *Pparg*$^{\Delta Lyz2}$ mice following IAV infection. Taken together, these data suggest that
246 PPAR-γ expression in AM, rather than in monocytes or monocyte-derived cells, is probably responsible
247 for the restriction of exaggerated pulmonary inflammation and the suppression of the development of
248 severe diseases following respiratory viral infection.
249

250 **Macrophage PPAR-γ promotes tissue repair**

251 Following the clearance of IAV, the inflammatory responses in the lung resolve and the damaged tissue
252 undergoing repair process to restore normal tissue homeostasis. AM are thought to be involved in the
253 tissue repair process following lung injury (32). We therefore examined whether PPAR-γ affects AM
254 tissue repair function. To this end, we isolated control or PPAR-γ-deficient AM from WT or *Pparg*$^{\Delta Lyz2}$
255 mice and performed Qiagen RT^{2}-PCR array to determine wound healing gene expression. We found that

PPAR-γ deficiency resulted in impaired expression of a large numbers of wound healing-related genes including epithelial and endothelial growth factors such as *Vegf*, *Egf* and *Fgf7* (Figure 6 A, B). A numbers of factors involved in tissue remodeling including *Mmp7*, *Mmp9* and *Timp1* were also decreased in PPAR-γ-deficient AM (Figure 6 A, B). These data suggested that PPAR-γ expression is important in regulating wound healing and tissue repair function of AM.

Therefore, we examined whether *Pparg*$^{\Delta Lyz2}$ mice had impaired tissue recovery *in vivo* following viral clearance. To this end, we examined lung histopathology with Hematoxylin and Eosin (H&E) staining of lung sections at 15 d.p.i., when infectious virus has been cleared from IAV infection (Figure 3C). We found that *Pparg*$^{\Delta Lyz2}$ mice still had significant higher proportions of the inflamed and/or damaged areas that were not properly repaired at day 15 p.i., when mice already recovered most of their lost weight (Figure 3B and 6 C). To further explore the roles of myeloid PPAR-γ in regulating lung inflammation resolution and tissue repair, we first examined airway inflammatory cell content (monocytes and neutrophils, reflection of lung inflammatory resolution). We found that *Pparg*$^{\Delta Lyz2}$ mice exhibited higher neutrophil numbers at 15 d.p.i., suggesting that *Pparg*$^{\Delta Lyz2}$ mice had impaired pulmonary inflammation resolution (Figure 6 D). We also measured total protein concentrations in the BAL (reflection of endothelial/epithelial leakage) at different days following IAV infection and observed that *Pparg*$^{\Delta Lyz2}$ mice had drastically higher protein levels in the BAL compared to those of control mice at 15 d.p.i (Figure 6 E). These data indicate that *Pparg*$^{\Delta Lyz2}$ mice had impaired inflammation resolution and decreased damage repair. In further support of this view, we examined alveolar type II (AT II) epithelial gene expression in the lungs of control and *Pparg*$^{\Delta Lyz2}$ mice as a surrogate of tissue recovery at 8, 10 or 15 d.p.i. We found that ATII specific genes, *Sftpb* and *Abca3*, were comparable between control and *Pparg*$^{\Delta Lyz2}$ lungs at 8 d.p.i. However, lungs of *Pparg*$^{\Delta Lyz2}$ mice exhibited lower *Sftpb* and *Abca3* expression compared to those of control mice at 10 or 15 d.p.i. (Figure 6 F), indicating that lungs of infected *Pparg*$^{\Delta Lyz2}$ mice had diminished ATII cell regeneration and lung recovery during viral clearance. Taken together, these data suggest that PPAR-γ promoted AM tissue repair function and myeloid-deficiency of PPAR-γ resulted in diminished inflammation resolution and impaired tissue recovery following IAV infection.

DISCUSSION

The transcriptional regulation of lung macrophage responses against respiratory viral infections is largely undefined. Here we identify that PPAR-γ expression in AM is vital for their proper responses during both IAV and RSV infection. PPAR-γ is an anti-inflammatory transcription factor able to antagonize NF-κb-mediated cytokine production constitutively and in response to TLR ligand stimulation (45). Consistent with the notion, we showed that PPAR-γ-deficient AM produced increased levels of both antiviral and pro-inflammatory cytokines in response to IAV and RSV infection. Notably, AM constitutively express high levels of PPAR-γ, which may help to maintain a tolerogenic environment in the lung during homeostasis. However, AM can also rapidly produce inflammatory cytokines following microbial challenge (17, 46). The down-regulation of PPAR-γ in AM may help the AM to rapidly respond to certain microbial challenges and provide beneficial functions under certain conditions. Nevertheless, the complete loss of PPAR-γ in macrophages caused exaggerated release of inflammatory mediators and enhanced disease development *in vivo* following IAV and RSV infections. These data suggest that PPAR-γ counter-regulates the pathogenic inflammatory responses *in vivo*, and acts to ensure the proper function of lung macrophages during respiratory viral infections.

The differential functions of AM and recruited monocyte/macrophage populations during homeostasis and disease conditions have only begun to be appreciated. During respiratory viral infections, circulating monocytes infiltrate the lungs in a CCR2-dependent manner and can give rise to exudate or inflammatory macrophages at the site of infection (42). These CCR2-dependent inflammatory monocytes and monocyte-derived cells have been associated with the development of immunopathology, although these cells also contribute to the normal antiviral responses as the blockage of their migration to the lung due to CCR2 inhibition or deficiency impaired and/or delayed host viral clearance during RSV and IAV infections (31, 40-42, 44). Notably, CCR2 deficiency or CCR2 blockade did not significantly change overall host morbidity in PPAR-γ sufficient or deficient background in our experimental system than what was reported before(31, 41), in which CCR2 deficiency significantly diminished host morbidity and mortality. Variations in infection schemes, virus stocks and/or microbiota (46) may contribute to the different results observed. However, our results are supported by the findings of Aldridge et al (40), in which *Ccr2*$^{-/-}$ deficient mice exhibited similar morbidity and mortality as WT mice following IAV infection.

318 In contrast, lung resident AM are often beneficial to the host during respiratory viral infections as AM
319 depletion impairs host antiviral responses with concomitant development of severe lung injury during
320 respiratory viral infections (25-31). However, AM do release inflammatory mediators following viral
321 infections and thus may contribute to the development respiratory inflammation and/or injury if their
322 responses are not tightly regulated. Multiple lines of evidence present in this study suggest that PPAR-γ
323 expression in AM rather than in monocytes and/or monocyte-derived cells is important in controlling host
324 inflammation and subsequent disease development. First, AM expressed high levels of PPAR-γ compared
325 to monocytes and monocyte-derived cells. Furthermore, sorted AM rather than monocytes or monocyte-
326 derived cells exhibited increased inflammatory responses. Finally, disruption of monocyte recruitment
327 into the lungs by using anti-CCR2 or genetic CCR2 deletion did not majorly impact the outcome of IAV
328 infection in WT and myeloid PPAR-γ deficient mice, suggesting that PPAR-γ expression in monocytes
329 may be dispensable for the regulation of the development of severe diseases following respiratory viral
330 infection. Interestingly, PPAR-γ expression also regulated the wound healing function of AM and tissue
331 recovery through the promotion of various growth factors and tissue remodeling factors. Notably, PPAR-γ
332 deficiency did not result in decreased M2 gene expression in AM with or without IAV or RSV infection,
333 suggesting that PPAR-γ may regulate AM repair function independent of M2 polarization. Thus, PPAR-γ
334 is vital for the proper function of AM during respiratory viral infection by restricting their inflammatory
335 features and simultaneously promoting their repair roles.
336
337 Type I IFNs are widely recognized as host-beneficial, anti-viral cytokines. They lead to the transcription
338 of IFN-stimulated genes that aim to eliminate the virus and prevent its spread by promoting anti-viral
339 state in nearby cells (47). However, type I IFNs are also the key initiators of pulmonary inflammatory
340 responses during respiratory viral infections and thus their actions must also be finely balanced to
341 maximize viral clearance while inflicting minimal damage to the tissue (48). Indeed, the exaggerated
342 production of type I IFNs have been implicated in the development of exuberant pulmonary inflammation,
343 severe host morbidity and mortality following respiratory viral infections (44, 49, 50). In this report, the
344 enhanced type I IFN production was observed in PPAR-γ deficient AM, but the absence of PPAR-γ in
345 AM resulted in significantly increased viral titers at four days following IAV infection, suggesting that
346 the enhanced production of type I IFNs by PPAR-γ-deficient AM was not sufficient to diminish viral
347 replication in the lungs. The exact reasons underlying the phenomenon warrant further investigation.
348 Nevertheless, given the potential inflammatory function of type I IFNs, it is possible that the altered
349 production of type I IFNs along with the dysregulated inflammatory cytokine production in PPAR-γ
350 deficient AM contribute to the severe outcome of IAV infection in the myeloid PPAR-γ deficient mice.

In summary, our findings have uncovered critical roles of PPAR-γ in regulating inflammatory responses of AM, the development of acute host disease and the proper restoration of tissue homeostasis following respiratory viral infections. Further studies are warranted to examine the therapeutic potential of modalities that can specifically modulate the expression of PPAR-γ in AM for the treatment of severe respiratory viral infections and their associated pathologies.

MATERIALS AND METHODS

Mouse and infection. WT C57/BL6 mice were purchased from the Jackson Laboratory. Lyz2-cre, CD11c-cre, *Pparg*$^{fl/fl}$, R26R-eYFP, *Ccr2*$^{-/-}$ were purchased from the Jackson Laboratory and bred in house. *Pparg*$^{\Delta Lyz2}$ mice were generated by crossing *Pparg*$^{fl/fl}$ mice with Lyz2-cre mice. Pparg$^{\Delta CD11c}$ were generated by crossing *Pparg*$^{fl/fl}$ mice with CD11c-cre mice. *Ccr2*$^{-/-}$ *Pparg*$^{fl/fl}$ and *Ccr2*$^{-/-}$ *Pparg*$^{\Delta Lyz2}$ mice were generated by crossing *Pparg*$^{fl/fl}$ or Pparg$^{\Delta Lyz2}$ mice with *Ccr2*$^{-/-}$ mice. Lyz2-cre R26R-eYFP reporter mice were generated by crossing R26R-eYFP mice with Lyz2-cre mice. All mice housed in a specific pathogen-free environment. For IAV infection, influenza A/PR8/34 strain (~200 pfu/mouse) was diluted in FBS-free DMEM media (Corning) on ice and inoculated in anesthetized mice through intranasal route as described before (51). Host mortality was determined based on humane endpoint (more than 30% weight loss or moribund) or deaths before humanely sacrifice. For RSV infection, RSV (strain line 19, ~5×10^6 pfu/mouse) was diluted in FBS-free DMEM media (Corning) on ice and inoculated in anesthetized mice through intranasal route as described (52).

AM culture and infection *in vitro*. AM were obtained from BAL. Briefly, alveolar lavages were pooled from BAL washes from 3-5 mice (PBS with 2 mM EDTA) and stored on ice. Red blood cell lysis was then performed in ACK lysis buffer (0.15 M NH_4Cl, 1 mM $KHCO_3$, 0.1 mM Na_2EDTA, pH 7.2) at room temperature for 2 min. Freshly isolated cells were rested in complete medium (RPMI-1640, 10% FBS, 1% Pen/Strep) for 4 h at 37℃ and 5% CO_2. The non-adherent cells were discarded, and the plates were rinsed with warm PBS. For AM infection *in vitro*, seeded cells were infected with or without 10 MOI of IAV PR8 virus or RSV line 19 as indicated in the text for 1 hour and then cultured for overnight. For AM IFN treatment *in vitro*, 10^5 AM were plated in 12-well plate and treated with 50 ng/ml IFN-α (BioLegend) or vehicle overnight in the presence of recombinant GM-CSF to keep AM alive (Biolegend, 10ng/ml). Cell lysates were analyzed by quantitative RT-PCR or western blot.

Quantitative RT-PCR. mRNA from cultured AM (pooled from multiple mice), *in vivo* sorted AM (pooled from multiple mice) or homogenates from individual lungs as indicated in the text was isolated with Total RNA purification kit (Sigma) and treated with DNase I (Invitrogen). Random primers (Invitrogen) and MMLV reverse transcriptase (Invitrogen) were used to synthesize first-strand cDNAs from equivalent amounts of RNA from each sample. RT-PCR was performed with Fast SYBR Green PCR Master Mix (Applied Biosystems). qPCR was conducted in duplicates in QuantStudio3 (Applied Bioscience). Data were generated with the comparative threshold cycle (Delta CT) method by normalizing to hypoxanthine phosphoribosyltransferase (HPRT). Sequences of primers used in the studies are provided as follows. *Abca3:* TTCTGGTTCTCCGCTCTGTT, GTACATGAGGGGGATGATGG.

Arg1: CAATGAAGAGCTGGCTGGTG, TGAGCATCCACCCAAATGAC.
Ccl2: GTCACCAAGCTCAAGAGAGAGGTC, CCTACAGAAGTGCTTGAGGTGGTT.
Hprt: CTCCGCCGGCTTCCTCCTCA, ACCTGGTTCATCATCGCTAATC.
Ifna4: TCCATCAGCAGCTCAATGAC, AGGAAGAGAGGGCTCTCCAG.
Ifnb1: TCCACCAGCAGACAGTGTT, CTTTGCACCCTCCAGTAATAGC.
Il1b: GGGCCTCAAAGGAAAGAATC, TACCAGTTGGGGAACTCTGC.
Pparg: TGCCAGTTTCGATCCGTAGA, ATGAATCCTTGGCCCTCTGA.
Retnla: TGCCCTGCTGGGATGACTGCT, GGACAGTTGGCAGCAGCGGG.
Sftpb: CTGTGCCAAGAGTGTGAGGA, TTGGGGTTAATCTGGCTCTG.
Tnf: CATGCGTCCAGCTGACTAAA, TCCCCTTCATCTTCCTCCTT.

RT^2 Profiler PCR Array. Total RNA from lung tissue or AM was extracted as described above. Equal amount of total RNA was used for the synthesis of first strand cDNA with kit from Qiagen. First strand cDNA was mixed with 2xFast SYBR Green Master Mix (Applied Bioscience) and water in a formula directed in the manual. 25 µl of the mixture was added into each well of the 96 well plate provided by manufacture. The wells in the plate include different primers in each well to detect 84 target genes, housekeeping genes, negative and positive control genes. qPCR was conducted in QuantStudio3 (Applied Bioscience). Obtained raw data was analyzed in software provided by Qiagen (accessible online on the website of Qiagen). Following the instruction step by step, upload Excel file, designating control group, select housekeeping gene to normalize result and calculate the relative expression quantity.

Cell depletion. For monocyte depletion, mice were treated intraperitoneally (i.p.) with anti-CCR2 antibody (clone: MC21, 25 µg/mouse in 200 µl of PBS)(53) or control IgG daily from day 0 to day 6.

Lung histopathology. Following euthanasia, mice were perfused with PBS (10 mL) via the right ventricle. 10% paraformaldehyde (PF) was then gently instilled into the lung and left inflated for 1 minute before excising and moving lobe to 10% PF for 48 hours followed by transfer to ethanol (70%). Samples were shipped to Mayo Clinic Histology Core Lab (Scottsdale, AZ) where they were embedded in paraffin and 5 um sections were cut for Hematoxylin and eosin stain. To quantify percent of inflamed or disrupted alveolar area, H&E slides were scanned through the Aperio whole slide scanning system and exported to image files. Computer-based image analysis was performed using the Image J software (NIG, Bethesda, MD, USA). We first determined the total lung area by converting the image into gray scale followed with red highlighting through the adjustment of the Threshold. For determination of the inflamed and disrupted area, color images were split into single channels. We then used the green channel, highlighted the

460 inflamed areas in red by adjusting the Threshold and measured the areas based on pixel. The percentages
461 of disrupted and inflamed lung areas were calculated based on the ratio of highlighted disrupted areas to
462 the total lung area in each lung section.
463
464 **Western Blot analysis.** Same numbers of cultured or FACS-sorted AM were lysed in lysis buffer
465 (62.5mM Tris-HCL (pH 6.8), 2% SDS and 10% glycerol) with a protease inhibitor cocktail (Roche). The
466 lysates were then separated by SDS-PAGE and transferred to Immuno-Blot Nitrocellulose Membrane
467 (Bio-Rad,). The membranes were blocked with 5% non-fat milk in 20 mM Tris (pH 7.5), 0.5 M NaCl and
468 0.05% Tween 20 (TBST) for 1h at room temperature (RT), followed by incubation with primary Ab
469 against PPAR-γ (1:1000, Cell Signaling Technology) or β-actin (1:5000, Santa Cruz Biotechnology)
470 overnight at 4°C. After washing with TBST buffer, membranes were incubated with goat anti-rabbit or
471 anti-mouse secondary Ab (Promega). Peroxidase activity was detected with enhanced
472 chemiluminesecence (ECL).
473
474 **Chromatin Immunoprecipitation (ChIP).** AM were obtained from the lung of naïve WT C57BL6 mice,
475 using anti-CD169 magnetic beads, as recommended by the manufacturer (Miltenyi Biotec). AM were
476 cultured in complete medium supplemented with 10 ng/ml GM-CSF in the presence of 50 ng/ml IFN-α
477 (BioLegend) or vehicle overnight. Then the cells were subjected to ChIP assay as previously described
478 (54). In brief, $8x10^6$ AM were crosslinked for 10 min at 37℃ by the addition of 1% freshly made
479 formaldehyde. Fixed cells were pelleted at 4℃ and washed with ice-cold PBS. The cells were lysed with
480 SDS lysis buffer (1% SDS, 10mM EDTA, 50mM Tris, pH 8.1) containing protease inhibitors (Roche) on
481 ice for 10 min and sonicated to an average size of 200-500bp. After sonication, samples were centrifuged
482 at 13,000 rpm for 10 min at 4℃ and 5% of sonicated cell extracts were saved as input. The resulting
483 whole-cell extract was incubated with Protein A/G Agarose (Santa Cruz) for 1h at 4℃. Precleared extracts
484 were then incubated with 60 ul of Protein A/G Agarose (Santa Cruz) for ChIP with 5μg of the appropriate
485 antibody overnight at 4℃. STAT1 ChIP antibody (clone D1K9Y) was from Cell Signaling. After
486 overnight incubation, beads were washed once with low salt immune complex wash buffer (0.1% SDS, 1%
487 Triton X-100, 2 mM EDTA, 20 mM Tris-HCL pH 8.1, 150 mM NaCl), once with high salt immune
488 complex wash buffer (0.1% SDS, 1% Triton X-100, 2 mM EDTA, 20 mM Tris-HCL pH 8.1, 500 mM
489 NaCl), once with LiCl wash buffer (10 mM Tris-HCl pH 8.1, 1 mM EDTA, 250 mM LiCl, 1% NP-40),
490 and twice with TE wash buffer (10 mM Tris-HCl pH 8.0, 1 mM EDTA). DNA was eluted in freshly
491 prepared elution buffer (1% SDS, 0.1M NaHCO3). Cross-links were reversed by overnight incubation
492 with 5 M NaCl at 65℃. RNA and protein were digested using RNase A and proteinase K (Roche),

493 respectively and DNA was purified by Qiagen MinElute PCR Purification kit according to the
494 manufacturer's instructions. The immunoprecipitated DNA was analyzed by quantitative real-time PCR
495 and normalized relative to input DNA amount. Primers were designed to a segment that was centered on
496 the PPAR-γ coverage regions. Primers used in this study are listed in as follows. Realtime PCR data is
497 represented as fold levels over control. Primers sequence are as following. *Pparg* -4.3k:
498 TGGAATGAAAGAATCCTCCAA, GTTGGTGCCACATGGATTTT. *Pparg* -16.8k:
499 GCAGATTTGTGCCAAGAACA, TGCAGCCGCTGAATAAATAC.
500
501 **ELISA analysis of BAL cytokines.** 50 µl of each BAL sample was analyzed with the ELISA using
502 commercially available kits for mouse IL-1β, CCL2 and TNF-α (Biolegend) following the manufacturer's
503 protocol. The VERSAmax microplate reader (Molecular Devices) was used for colorimetric
504 quantification and analysis at 450nM wavelength.
505
506 **BCA protein assay.** BCA protein assay kit was obtained from Thermo Scientific. 2µl of each BALF
507 sample was used. VERSAmax microplate reader (Molecular Devices) was used for colorimetric
508 quantification and analysis at 570nm wavelength.
509
510 **Plaque Assay.** IAV plaque assays were performed as described before (55). Briefly, MDCK cells were
511 grown in 6-well plates and incubated with series dilution of BALF for 1 h. The plates were then overlaid
512 with low melting temperature agarose (0.6 %) in MEM with BSA and trypsin and cultured for 3 days in
513 37°C incubator. Plates were then fixed with formaldehyde and virus plaques were visualized with the
514 staining of neutral red.
515
516 **FACS analysis.** Fluorescence-conjugated FACS Abs were purchased from Biolegend, BD Biosciences or
517 eBioscience. Ab clones are provided. We defined cell populations based on following cell surface markers:
518 AM ($CD11c^+$ Siglec F^+ $CD11b^{low}$), Neutrophils ($CD11b^+$ $Ly6G^+$), total $CD11b^+$ Monocyte/Macrophage
519 population ($Ly6G^-$ Siglec F^- $CD11b^+$), Monocytes ($Ly6G^-$ Siglec F^- $CD11b^+$ $Ly6C^+$), NP_{366} tetramer$^+$ cells
520 ($CD8^+$ NP_{366}-tet$^+$), PA_{224} tetramer$^+$ cells ($CD8^+$ PA_{224}-tet$^+$). Samples were collected on FACS Attune or
521 FACS Attune NXT flow cytometer (Life technologies) and analyzed using Flow Jo software (Tree Star).
522
523 **Statistical analysis.** Data are mean ± SEM of values from individual mice (*in vivo* experiments).
524 Unpaired two-tailed Student's t-test (two group comparison), Multiple t-tests (weight loss) or Logrank

test (survival study) were used to determine statistical significance by GraphPad Prism software. We consider P values < 0.05 as significant.

ACKNOWLEDGMENTS

We thank Thomas Braciale and Khashayarsha Khazaie for critical reading of the manuscript. We thank NIH tetramer facility for providing IAV-specific tetramers and Mayo flow cytometry core for help of cell sorting. This work was supported by the US National Institutes of Health grants (RO1 HL126647, AG047156, AI112844, R21 AI099753 to J.S.; R01 AI095282 and AI129241 to M.H.K.; RO1 HL62150 to A.H.L.; T32 AG049672 to N.P.G.), Kogod Aging Center High Risk Pilot Grant to J.S. and Huvis Foundation grant to A.H.L.

REFERENCES

1. **Openshaw PJM, Chiu C, Culley FJ, Johansson C.** 2017. Protective and Harmful Immunity to RSV Infection. Annu Rev Immunol **35:**501-532.

2. **Zhou H, Thompson WW, Viboud CG, Ringholz CM, Cheng PY, Steiner C, Abedi GR, Anderson LJ, Brammer L, Shay DK.** 2012. Hospitalizations associated with influenza and respiratory syncytial virus in the United States, 1993-2008. Clin Infect Dis **54:**1427-1436.
3. **Molinari NA, Ortega-Sanchez IR, Messonnier ML, Thompson WW, Wortley PM, Weintraub E, Bridges CB.** 2007. The annual impact of seasonal influenza in the US: measuring disease burden and costs. Vaccine **25:**5086-5096.
4. **Doherty PC, Turner SJ, Webby RG, Thomas PG.** 2006. Influenza and the challenge for immunology. Nat Immunol **7:**449-455.
5. **Thomas PG, Keating R, Hulse-Post DJ, Doherty PC.** 2006. Cell-mediated protection in influenza infection. Emerg Infect Dis **12:**48-54.
6. **Hussain M, Galvin HD, Haw TY, Nutsford AN, Husain M.** 2017. Drug resistance in influenza A virus: the epidemiology and management. Infect Drug Resist **10:**121-134.
7. **Braciale TJ, Sun J, Kim TS.** 2012. Regulating the adaptive immune response to respiratory virus infection. Nat Rev Immunol **12:**295-305.
8. **Sun J, Braciale TJ.** 2013. Role of T cell immunity in recovery from influenza virus infection. Curr Opin Virol **3:**425-429.
9. **de Jong MD, Simmons CP, Thanh TT, Hien VM, Smith GJ, Chau TN, Hoang DM, Chau NV, Khanh TH, Dong VC, Qui PT, Cam BV, Ha do Q, Guan Y, Peiris JS, Chinh NT, Hien TT, Farrar J.** 2006. Fatal outcome of human influenza A (H5N1) is associated with high viral load and hypercytokinemia. Nat Med **12:**1203-1207.
10. **Kobasa D, Jones SM, Shinya K, Kash JC, Copps J, Ebihara H, Hatta Y, Kim JH, Halfmann P, Hatta M, Feldmann F, Alimonti JB, Fernando L, Li Y, Katze MG, Feldmann H, Kawaoka Y.** 2007. Aberrant innate immune response in lethal infection of macaques with the 1918 influenza virus. Nature **445:**319-323.
11. **Lavin Y, Mortha A, Rahman A, Merad M.** 2015. Regulation of macrophage development and function in peripheral tissues. Nat Rev Immunol **15:**731-744.
12. **Geissmann F, Mass E.** 2015. A stratified myeloid system, the challenge of understanding macrophage diversity. Semin Immunol **27:**353-356.
13. **Geissmann F, Gordon S, Hume DA, Mowat AM, Randolph GJ.** 2010. Unravelling mononuclear phagocyte heterogeneity. Nat Rev Immunol **10:**453-460.
14. **Ginhoux F, Guilliams M.** 2016. Tissue-Resident Macrophage Ontogeny and Homeostasis. Immunity **44:**439-449.
15. **Perdiguero EG, Geissmann F.** 2016. The development and maintenance of resident macrophages. Nat Immunol **17:**2-8.
16. **Hussell T, Bell TJ.** 2014. Alveolar macrophages: plasticity in a tissue-specific context. Nat Rev Immunol **14:**81-93.
17. **Kopf M, Schneider C, Nobs SP.** 2015. The development and function of lung-resident macrophages and dendritic cells. Nat Immunol **16:**36-44.
18. **Guilliams M, De Kleer I, Henri S, Post S, Vanhoutte L, De Prijck S, Deswarte K, Malissen B, Hammad H, Lambrecht BN.** 2013. Alveolar macrophages develop from fetal monocytes that differentiate into long-lived cells in the first week of life via GM-CSF. J Exp Med **210:**1977-1992.
19. **Schneider C, Nobs SP, Kurrer M, Rehrauer H, Thiele C, Kopf M.** 2014. Induction of the nuclear receptor PPAR-gamma by the cytokine GM-CSF is critical for the differentiation of fetal monocytes into alveolar macrophages. Nat Immunol **15:**1026-1037.
20. **Yu X, Buttgereit A, Lelios I, Utz SG, Cansever D, Becher B, Greter M.** 2017. The Cytokine TGF-beta Promotes the Development and Homeostasis of Alveolar Macrophages. Immunity **47:**903-912 e904.
21. **Schneider C, Nobs SP, Heer AK, Hirsch E, Penninger J, Siggs OM, Kopf M.** 2017. Frontline Science: Coincidental null mutation of Csf2ralpha in a colony of PI3Kgamma-/- mice causes alveolar macrophage deficiency and fatal respiratory viral infection. J Leukoc Biol **101:**367-376.
22. **Deng W, Yang J, Lin X, Shin J, Gao J, Zhong XP.** 2017. Essential Role of mTORC1 in Self-Renewal of Murine Alveolar Macrophages. J Immunol **198:**492-504.

609 23. **Kawasaki T, Ito K, Miyata H, Akira S, Kawai T.** 2017. Deletion of PIKfyve alters alveolar macrophage
610 populations and exacerbates allergic inflammation in mice. EMBO J **36:**1707-1718.
611 24. **Todd EM, Zhou JY, Szasz TP, Deady LE, D'Angelo JA, Cheung MD, Kim AH, Morley SC.** 2016. Alveolar
612 macrophage development in mice requires L-plastin for cellular localization in alveoli. Blood **128:**2785-
613 2796.
614 25. **Laidlaw BJ, Decman V, Ali MA, Abt MC, Wolf AI, Monticelli LA, Mozdzanowska K, Angelosanto JM, Artis**
615 **D, Erikson J, Wherry EJ.** 2013. Cooperativity between CD8+ T cells, non-neutralizing antibodies, and
616 alveolar macrophages is important for heterosubtypic influenza virus immunity. PLoS Pathog **9:**e1003207.
617 26. **Schneider C, Nobs SP, Heer AK, Kurrer M, Klinke G, van Rooijen N, Vogel J, Kopf M.** 2014. Alveolar
618 macrophages are essential for protection from respiratory failure and associated morbidity following
619 influenza virus infection. PLoS Pathog **10:**e1004053.
620 27. **Kim HM, Lee YW, Lee KJ, Kim HS, Cho SW, van Rooijen N, Guan Y, Seo SH.** 2008. Alveolar macrophages
621 are indispensable for controlling influenza viruses in lungs of pigs. J Virol **82:**4265-4274.
622 28. **Purnama C, Ng SL, Tetlak P, Setiagani YA, Kandasamy M, Baalasubramanian S, Karjalainen K, Ruedl C.**
623 2014. Transient ablation of alveolar macrophages leads to massive pathology of influenza infection
624 without affecting cellular adaptive immunity. Eur J Immunol **44:**2003-2012.
625 29. **Kumagai Y, Takeuchi O, Kato H, Kumar H, Matsui K, Morii E, Aozasa K, Kawai T, Akira S.** 2007. Alveolar
626 macrophages are the primary interferon-alpha producer in pulmonary infection with RNA viruses.
627 Immunity **27:**240-252.
628 30. **Cardani A, Boulton A, Kim TS, Braciale TJ.** 2017. Alveolar Macrophages Prevent Lethal Influenza
629 Pneumonia By Inhibiting Infection Of Type-1 Alveolar Epithelial Cells. PLoS Pathog **13:**e1006140.
630 31. **Goritzka M, Makris S, Kausar F, Durant LR, Pereira C, Kumagai Y, Culley FJ, Mack M, Akira S, Johansson C.**
631 2015. Alveolar macrophage-derived type I interferons orchestrate innate immunity to RSV through
632 recruitment of antiviral monocytes. J Exp Med **212:**699-714.
633 32. **Gorski SA, Hufford MM, Braciale TJ.** 2012. Recent insights into pulmonary repair following virus-induced
634 inflammation of the respiratory tract. Curr Opin Virol **2:**233-241.
635 33. **Ahmadian M, Suh JM, Hah N, Liddle C, Atkins AR, Downes M, Evans RM.** 2013. PPARgamma signaling
636 and metabolism: the good, the bad and the future. Nat Med **19:**557-566.
637 34. **Odegaard JI, Ricardo-Gonzalez RR, Goforth MH, Morel CR, Subramanian V, Mukundan L, Red Eagle A,**
638 **Vats D, Brombacher F, Ferrante AW, Chawla A.** 2007. Macrophage-specific PPARgamma controls
639 alternative activation and improves insulin resistance. Nature **447:**1116-1120.
640 35. **Chawla A.** 2010. Control of macrophage activation and function by PPARs. Circ Res **106:**1559-1569.
641 36. **Moseley CE, Webster RG, Aldridge JR.** 2010. Peroxisome proliferator-activated receptor and AMP-
642 activated protein kinase agonists protect against lethal influenza virus challenge in mice. Influenza Other
643 Respir Viruses **4:**307-311.
644 37. **Darwish I, Mubareka S, Liles WC.** 2011. Immunomodulatory therapy for severe influenza. Expert Rev Anti
645 Infect Ther **9:**807-822.
646 38. **Cloutier A, Marois I, Cloutier D, Verreault C, Cantin AM, Richter MV.** 2012. The prostanoid 15-deoxy-
647 Delta12,14-prostaglandin-j2 reduces lung inflammation and protects mice against lethal influenza
648 infection. J Infect Dis **205:**621-630.
649 39. **Fedson DS.** 2013. Treating influenza with statins and other immunomodulatory agents. Antiviral Res
650 **99:**417-435.
651 40. **Aldridge JR, Jr., Moseley CE, Boltz DA, Negovetich NJ, Reynolds C, Franks J, Brown SA, Doherty PC,**
652 **Webster RG, Thomas PG.** 2009. TNF/iNOS-producing dendritic cells are the necessary evil of lethal
653 influenza virus infection. Proc Natl Acad Sci U S A **106:**5306-5311.
654 41. **Herold S, Steinmueller M, von Wulffen W, Cakarova L, Pinto R, Pleschka S, Mack M, Kuziel WA, Corazza**
655 **N, Brunner T, Seeger W, Lohmeyer J.** 2008. Lung epithelial apoptosis in influenza virus pneumonia: the
656 role of macrophage-expressed TNF-related apoptosis-inducing ligand. J Exp Med **205:**3065-3077.
657 42. **Lin KL, Suzuki Y, Nakano H, Ramsburg E, Gunn MD.** 2008. CCR2+ monocyte-derived dendritic cells and
658 exudate macrophages produce influenza-induced pulmonary immune pathology and mortality. J Immunol
659 **180:**2562-2572.

43. **Hashimoto D, Chow A, Noizat C, Teo P, Beasley MB, Leboeuf M, Becker CD, See P, Price J, Lucas D, Greter M, Mortha A, Boyer SW, Forsberg EC, Tanaka M, van Rooijen N, Garcia-Sastre A, Stanley ER, Ginhoux F, Frenette PS, Merad M.** 2013. Tissue-resident macrophages self-maintain locally throughout adult life with minimal contribution from circulating monocytes. Immunity **38:**792-804.
44. **Channappanavar R, Fehr AR, Vijay R, Mack M, Zhao J, Meyerholz DK, Perlman S.** 2016. Dysregulated Type I Interferon and Inflammatory Monocyte-Macrophage Responses Cause Lethal Pneumonia in SARS-CoV-Infected Mice. Cell Host Microbe **19:**181-193.
45. **Gautier EL, Chow A, Spanbroek R, Marcelin G, Greter M, Jakubzick C, Bogunovic M, Leboeuf M, van Rooijen N, Habenicht AJ, Merad M, Randolph GJ.** 2012. Systemic analysis of PPARgamma in mouse macrophage populations reveals marked diversity in expression with critical roles in resolution of inflammation and airway immunity. J Immunol **189:**2614-2624.
46. **Ichinohe T, Pang IK, Kumamoto Y, Peaper DR, Ho JH, Murray TS, Iwasaki A.** 2011. Microbiota regulates immune defense against respiratory tract influenza A virus infection. Proc Natl Acad Sci U S A **108:**5354-5359.
47. **Garcia-Sastre A, Biron CA.** 2006. Type 1 interferons and the virus-host relationship: a lesson in detente. Science **312:**879-882.
48. **Teijaro JR, Walsh KB, Cahalan S, Fremgen DM, Roberts E, Scott F, Martinborough E, Peach R, Oldstone MB, Rosen H.** 2011. Endothelial cells are central orchestrators of cytokine amplification during influenza virus infection. Cell **146:**980-991.
49. **Teijaro JR.** 2015. The role of cytokine responses during influenza virus pathogenesis and potential therapeutic options. Curr Top Microbiol Immunol **386:**3-22.
50. **Davidson S, Crotta S, McCabe TM, Wack A.** 2014. Pathogenic potential of interferon alphabeta in acute influenza infection. Nat Commun **5:**3864.
51. **Sun J, Madan R, Karp CL, Braciale TJ.** 2009. Effector T cells control lung inflammation during acute influenza virus infection by producing IL-10. Nat Med **15:**277-284.
52. **Yao S, Jiang L, Moser EK, Jewett LB, Wright J, Du J, Zhou B, Davis SD, Krupp NL, Braciale TJ, Sun J.** 2015. Control of pathogenic effector T-cell activities in situ by PD-L1 expression on respiratory inflammatory dendritic cells during respiratory syncytial virus infection. Mucosal Immunol **8:**746-759.
53. **Mack M, Cihak J, Simonis C, Luckow B, Proudfoot AE, Plachy J, Bruhl H, Frink M, Anders HJ, Vielhauer V, Pfirstinger J, Stangassinger M, Schlondorff D.** 2001. Expression and characterization of the chemokine receptors CCR2 and CCR5 in mice. J Immunol **166:**4697-4704.
54. **Yao S, Buzo BF, Pham D, Jiang L, Taparowsky EJ, Kaplan MH, Sun J.** 2013. Interferon regulatory factor 4 sustains CD8(+) T cell expansion and effector differentiation. Immunity **39:**833-845.
55. **Huprikar J, Rabinowitz S.** 1980. A simplified plaque assay for influenza viruses in Madin-Darby kidney (MDCK) cells. J Virol Methods **1:**117-120.

FIGURE LEGENDS

Figure 1. IAV down-regulates PPAR-γ expression in AM.

A. Comparison of the expression of 84 transcription factors in AM (isolated and pooled from at least 3 mice) with or without IAV (IAV) infection for overnight *in vitro* by RT^2 Profiler PCR array. Dotted line: fold cutoff of gene expression (1.5 fold). Red dots, genes up-regulated following IAV infection. Green dots, genes down-regulated following IAV infection.

B. List of up- or down-regulated transcription factors in AM (isolated and pooled from at least 3 mice) following IAV infection *in vitro* for overnight by RT^2 Profiler PCR array.

C. Relative expression of *Pparg* in AM (isolated and pooled from at least 3 mice) with or without IAV infection for overnight *in vitro* by qRT-PCR.

D. Western blot analysis of PPAR-γ levels in AM (isolated and pooled from at least 3 mice) with or without IAV infection for overnight. Bar graph represents relative density of PPAR-γ band pooled from three independent experiments.

E. Relative expression of *Pparg* in sorted AM isolated from non-infected (day 0) or IAV-infected mice at 4, 6, 10 or15 p.i

F. Western blot analysis of PPAR-γ expression *ex vivo* in AM (isolated and pooled from at least 3 mice) isolated from non-infected (day 0) or IAV-infected lungs (6 d.p.i.). Bar graphs represent relative density of PPAR-γ band pooled from three independent experiments.

G. Western blot analysis of PPAR-γ expression in AM (isolated and pooled from at least 3 mice) with or without IFN-α treatment for overnight. Bar graph represent relative density of PPAR-γ band pooled from three independent experiments.

H. Relative expression of *Pparg* in AM (isolated and pooled from at least 3 mice) with or without IAV infection in the presence or absence of α-IFNAR1 for overnight *in vitro* by qRT-PCR.

I. STAT1 binding to *Pparg* loccus in AM following overnight IFN-α treatment *in vitro* was determined through ChIP (pooled from n>20 mice). Numbers in Red are distances of the binding sites to start codon.

Data are representative of two to three independent experiments. *, $P < 0.05$.

Figure 2. PPAR-γ suppresses antiviral inflammation, but not regulates M2 genes following infection

A. Airway AM percentages and CD11b expression on AM from control ($Pparg^{fl/fl}$) or $Pparg^{\Delta CD11c}$ mice, and control or $Pparg^{\Delta Lyz2}$ mice.

B. Western blot of PPAR-γ expression in sorted AM (isolated and pooled from 2-3 mice) from control ($Pparg^{fl/fl}$) or $Pparg^{\Delta Lyz2}$ mice at 0 and 3 d.p.i.

C. qRT-PCR analysis of *Ifna4*, *Ifnb1*, *Il1b*, *Tnf*, *Ccl2*, *Retnla* and *Arg1* expression in AM (isolated and pooled from 3 mice) from control ($Pparg^{fl/fl}$) or $Pparg^{\Delta Lyz2}$ mice following IAV infection *in vitro* for overnight.

D. Control or $Pparg^{\Delta Lyz2}$ mice were infected with IAV. *Ifna4*, *Ifnb1*, *Tnf*, *Ccl2*, *Retnla* and *Arg1* gene expression in AM (isolated and pooled from 2-3 mice) of control or $Pparg^{\Delta Lyz2}$ mice at day 1 and 3 p.i.

Data are representative of at least two independent experiments. *, $P < 0.05$.

Figure 3. Myeloid PPAR-γ suppresses host mortality, morbidity and pulmonary inflammation.

Control or $Pparg^{\Delta Lyz2}$ mice were infected with IAV.

A. Host mortality (% survival) was monitored.

B. Host morbidity (% initial weight) was monitored.

C. Airway IAV titers (pfu assay) were determined at day 4, 7, 10 or 15 p.i..

D. Lung IAV-specific PA_{224} and NP_{366} tetramer$^+$ $CD8^+$ T cells at day 7, 10 and 15 p.i.

E. CCL2 and TNF-α levels in the BAL were quantified by ELISA at day 1, 3, 7, 10 or 15 p.i.

F. Comparison of the expression of 84 inflammation-related genes in lungs from control or $Pparg^{\Delta Lyz2}$ mice at day 10 p.i. by RT^2 Profiler PCR array. Dotted line: 1.5 fold difference cutoff. Red dots, genes up-regulated in the lungs of $Pparg^{\Delta Lyz2}$ mice. Green dots, genes down-regulated in the lungs of $Pparg^{\Delta Lyz2}$ mice.

Data are representative of at least two independent experiments (n=3-6 mice per group) except A, B, C (pooled data from 2-6 experiments). *, $P < 0.05$.

Figure 4. Myeloid PPAR-γ suppresses pulmonary inflammation during RSV infection.

A. qRT-PCR analysis of *Ifna4*, *Ifnb1*, *Il1b*, *Tnf*, *Ccl2*, *Retnla* and *Arg1* expression in AM (isolated and pooled from at least 3 mice) from control ($Pparg^{fl/fl}$) or $Pparg^{\Delta Lyz2}$ mice following RSV infection (10 MOI) *in vitro* for overnight.

B-D. Control ($Pparg^{fl/fl}$) or $Pparg^{\Delta Lyz2}$ mice were infected with RSV.

B. Host morbidity (% initial weight) was monitored daily.

C. Numbers of lung neutrophils or monocytes at 4 d.p.i.

D. BAL TNF and IL-1β concentrations were determined through ELISA at 4 d.p.i.

Data are representative of at least two independent experiments (n=3-4 mice per group) except B (pooled data from 2 experiments). *, $P < 0.05$.

Figure 5. PPAR-γ expression in resident alveolar macrophages is likely required for the suppression of host morbidity

A. Lyz2-cre gene recombination in AM, neutrophils and CD11b^{+} monocytes/macrophages is reported by % eYFP expression following crossing with R26R-eYFP reporter mice.

B. Western blot analysis of PPAR-γ protein expression in sorted AM, CD11b^{+} monocytes/macrophages and neutrophils in the lungs from naïve WT mice (pooled from 3 mice).

C. *Tnf* and *Ccl2* expression in indicated cell populations in the lungs of control (*Pparg*$^{fl/fl}$) or *Pparg*$^{\Delta Lyz2}$ mice at day 1 and 3 p.i. (pooled from 2-3 mice per group).

D. *Ccr2*$^{-/-}$ *Pparg*$^{fl/fl}$ and *Ccr2*$^{-/-}$ *Pparg* $^{\Delta Lyz2}$ mice were infected with IAV. Host morbidity (% initial weight) was monitored.

E. WT mice were infected with IAV and treated with control IgG or MC21 mAb. % lung AM (upper panel) and monocytes (lower panel) in CD45^{+} Ly6G^{-} cells are depicted at 5 d.p.i.

F. Control (*Pparg*$^{fl/fl}$) and *Pparg*$^{\Delta Lyz2}$ mice were infected with IAV and treated with control IgG or MC21 mAb. Host morbidity (% initial weight) was monitored.

Data are representative of at least two to three independent experiments except C (pooled data from 3 experiments) and D. *, $P < 0.05$.

Figure 6. Macrophage PPAR-γ modulates inflammation resolution and tissue repair.

A. Comparison of the expression of 84 wound healing genes of AM isolated (pooled from 3 mice) from uninfected control or *Pparg*$^{\Delta Lyz2}$ mice *in vitro*. Dotted line: fold cutoff of gene expression (1.5 fold). Red dots, genes up-regulated in PPAR-γ-deficient AM. Green dots, genes down-regulated in PPAR-γ-deficient AM.

B. List of up- or down-regulated wound healing genes in AM (pooled from 3 mice) from control or *Pparg*$^{\Delta Lyz2}$ mice by RT^{2} Profiler PCR array.

C-F. Control (*Pparg*$^{fl/fl}$) or *Pparg*$^{\Delta Lyz2}$ mice were infected with IAV (n=3-4).

C. H&E staining of lung sections of control or *Pparg*$^{\Delta Lyz2}$ mice at day 15 p.i. Left panel, representative images. Right panel, quantification of percentages of inflamed and disrupted alveolar area in the lungs of control (*Pparg*$^{fl/fl}$) and *Pparg*$^{\Delta Lyz2}$ mice.

D. BAL neutrophil or monocyte numbers were enumerated at 15 d.p.i.

E. BAL total protein concentrations were determined at 1, 3, 7, 10 or 15 d.p.i.

F. *Sftpb* and *Abca3* gene expression in lungs from control or *Pparg*$^{\Delta Lyz2}$ mice at 8, 10 or 15 d.p.i.

Data are representative of at least two independent experiments, *, $P < 0.05$.

803

Figure 1

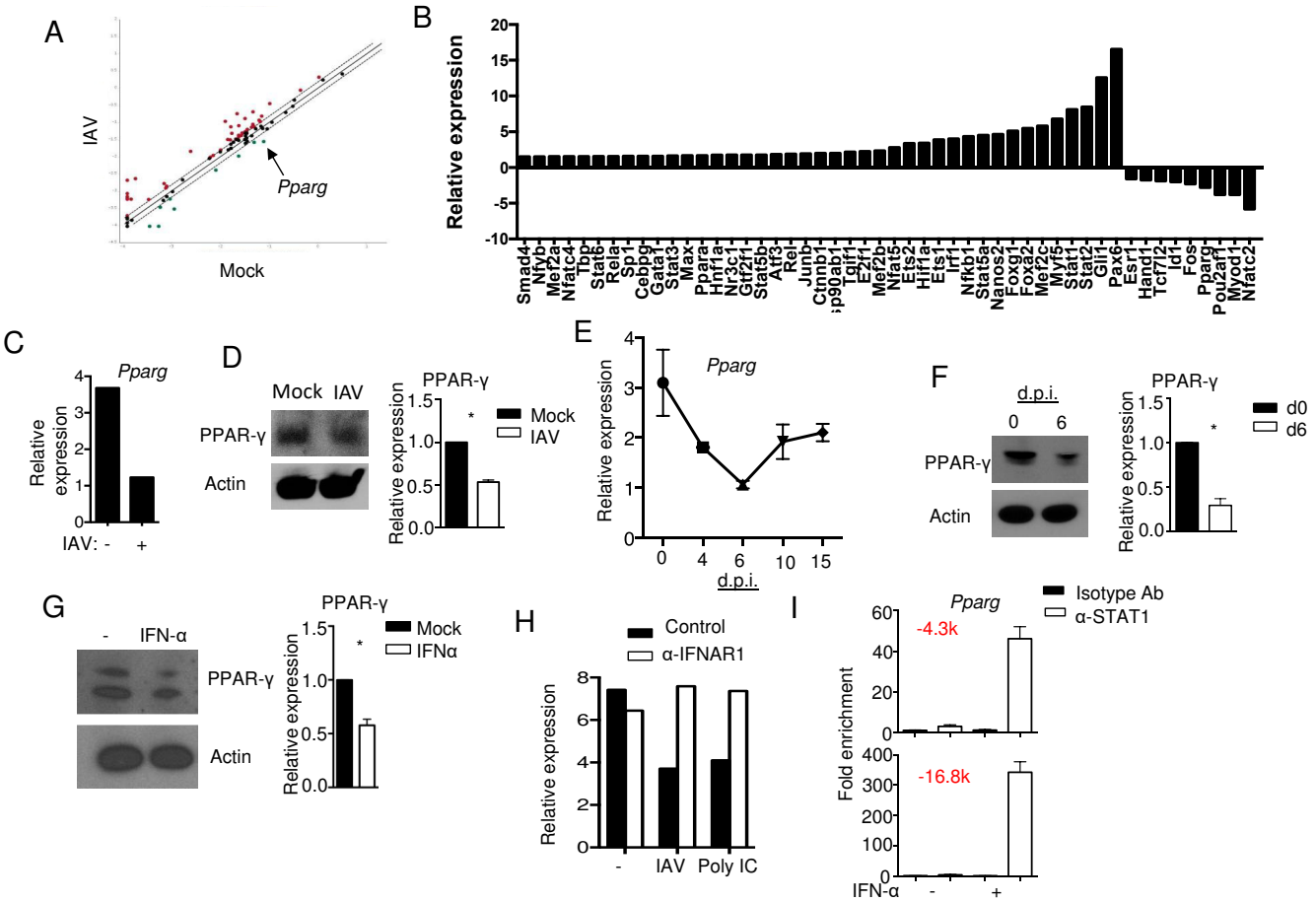

Figure 2

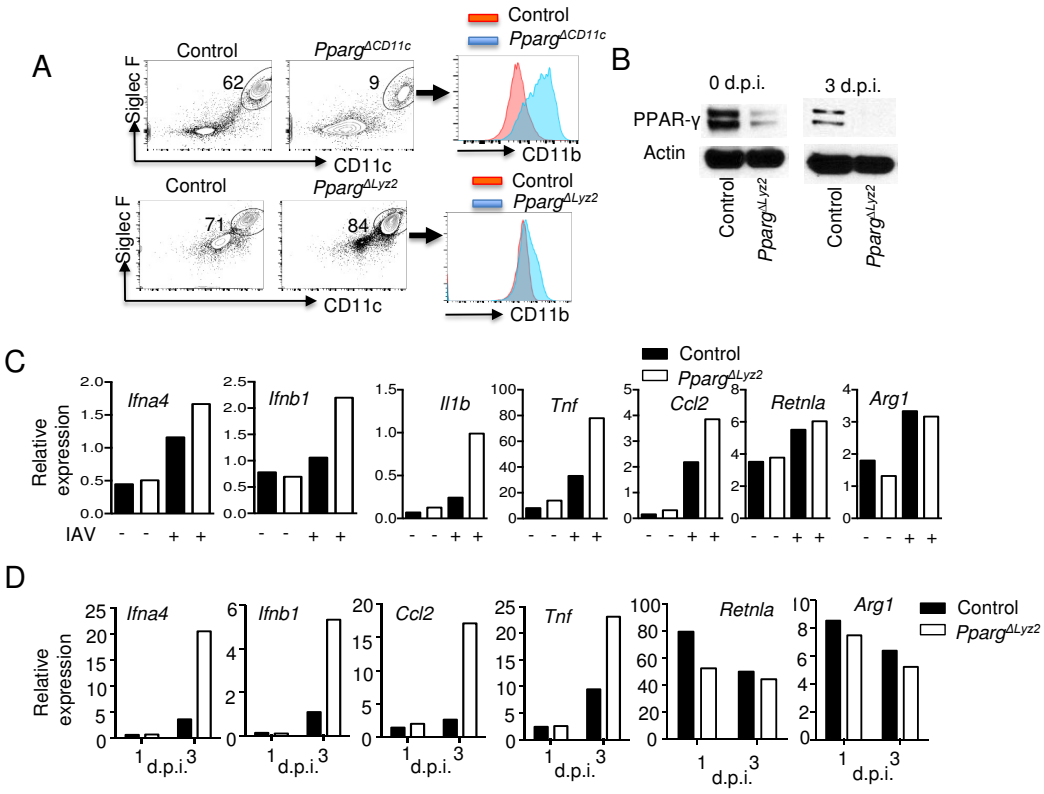

Figure 3

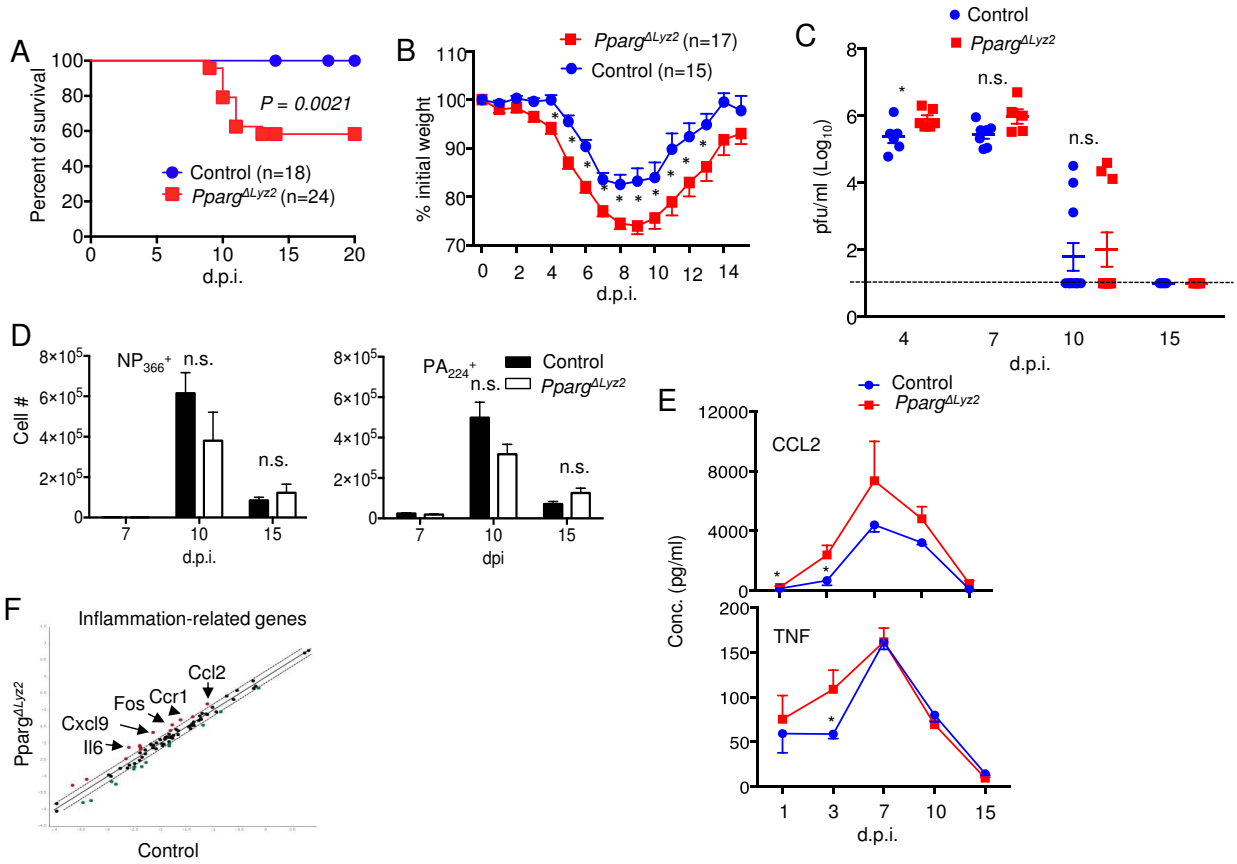

Figure 4

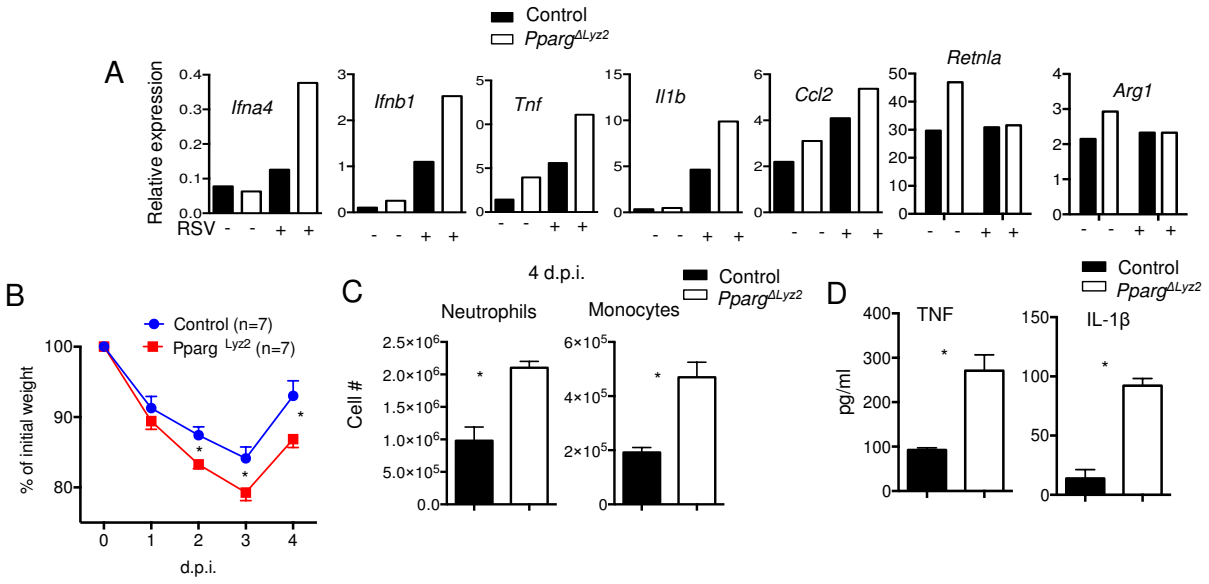

Figure 5

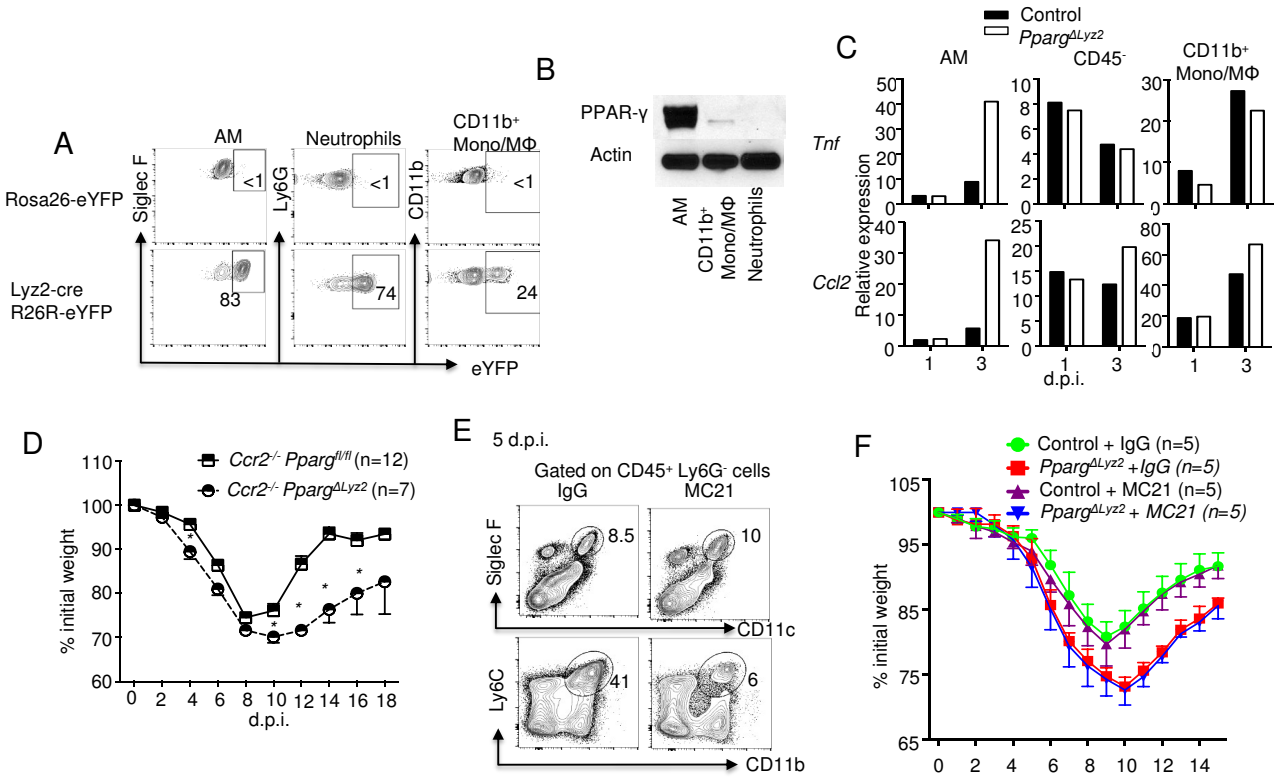

Figure 6